# Probing the Oligomeric State of Phospholamban Variants in Phospholipid Bilayers from Solid-State NMR Measurements of Rotational Diffusion Rates†

Eleri Hughes, Jonathan C. Clayton, and David A. Middleton*

*Faculty of Life Sciences, University of Manchester, P.O. Box 88, Sackville Street, Manchester M60 1QD, U.K.*

*Received August 16, 2004; Revised Manuscript Received December 23, 2004*

ABSTRACT: Phospholamban (PLB) is a small transmembrane protein that regulates calcium transport across the sarcoplasmic reticulum (SR) of cardiac cells. PLB self-associates into pentamers within sodium dodecyl sulfate (SDS) micelles, but the oligomeric status of PLB in SR membranes is not known. This work has shown that a mutant of PLB, with all native cysteine residues replaced by alanine (Ala-PLB), runs as a monomer on SDS−PAGE gels, in agreement with previous studies [Karim et al. (2000) *Biochemistry 39*, 10892−10897]. By contrast, a peptide representing the transmembrane domain of the cysteine-free mutant (TM-Ala-PLB) coexists as pentamers, dimers, and monomers on gels. Solid-state NMR methods were used to examine the size and heterogeneity of Ala-PLB and TM-Ala-PLB labeled with $^{13}C$ and $^{2}H$ in the transmembrane domain and incorporated into dimyristoylphosphatidylcholine (DMPC) bilayers. Wide line $^{2}H$ NMR and $^{13}C$ cross-polarization magic-angle spinning (CP-MAS) NMR spectra of Ala-PLB and TM-Ala-PLB revealed two distinct species of each of the proteins in the membranes. In the case of Ala-PLB one species was present initially and a second species emerged after 12 h. Measurements of $^{1}H-^{13}C$ dipolar couplings for the two species of Ala-PLB showed that the rotational diffusion of one species was relatively rapid, defined by a correlation time ($\tau_R$) of less than 10 $\mu$s, whereas the rotation of the other species was comparatively slow ($\tau_R \sim 60$ $\mu$s). These results suggest that although Ala-PLB runs as a monomer on gels, a mixture of different oligomeric forms of the protein, possibly monomers and pentamers, is present in DMPC bilayers. Caution must therefore be exercised in using SDS−PAGE to draw conclusions about the oligomeric state of PLB variants in lipid bilayers.

Phospholamban (PLB)[1] is a 52 amino acid transmembrane protein that contributes to the contraction-relaxation cycle of the heart by regulating calcium transport across the sarcoplasmic reticulum (SR) of cardiac muscle cells. The regulatory effect is achieved through a reversible interaction between PLB and the cardiac isoform of sarco(endo)plasmic reticulum calcium ATPase (SERCA2a), which lowers the affinity of the enzyme for calcium (*1*). On sodium dodecyl sulfate−polyacrylamide gel electrophoresis (SDS−PAGE) gels, wild-type (WT) PLB exhibits a pattern of oligomerization distributed mainly between populations of monomers (20%) and homopentamers (80%) (*2*). Consequently, it is believed that a dynamic equilibrium exists between pentameric and monomeric forms of PLB in sarcoplasmic reticulum (SR) membranes (*3*, *4*), although such species have not been confirmed directly. There is evidence that it is the monomeric form of PLB which interacts with SERCA2a and regulates calcium transport (*5*). Much of this evidence comes from experiments on mutants of PLB, which run as monomers on SDS−PAGE and suppress $Ca^{2+}$ affinity for $Ca^{2+}$-ATPase more strongly than does the wild-type protein (*5*−*7*). No physiological role has yet been attributed definitively to PLB pentamers.

Extensive mutational analysis of residues within the transmembrane domain of PLB (residues 23−52) has revealed the sites of interaction between PLB monomers that promote pentamer formation as assessed by SDS−PAGE. Mutations of residues L37, I40, L44, and I47 destabilize the pentameric state, while residues C36, L39, C41, L43, C46, V49, and L51 are only moderately sensitive to mutation (*8*). It is believed that C41 is located at a crucial site for maintaining the pentameric structure, since substitution of all three transmembrane cysteines with either Ala or Ser converts the protein to a monomeric form on SDS−PAGE gels (*9*). The general consensus is that WT PLB forms a pentameric coiled-coil structure, with close packing of L37, I40 L44, I47, and L51 in a leucine−isoleucine zipper motif. The five-helix bundle creates a central core lined with predominantly hydrophobic residues (*8*, *10*−*14*).

Gel electrophoresis is a valuable tool for assessing the propensity of PLB mutants to self-associate in SDS micelles, but it is unclear whether the behavior of PLB in detergent is predictive of its oligomeric status in biomembranes. Several

† The British Heart Foundation is acknowledged for a postdoctoral research fellowship (to E.H.) and a Ph.D. studentship (to J.C.C.). The BBSRC are thanked for support toward a 400 MHz NMR spectrometer under the Joint Research Equipment Initiative.

* To whom correspondence should be addressed. Tel: +44 161 2004217. Fax: +44 161 2360409. E-mail: david.a.middleton@manchester.ac.uk.

[1] Abbreviations: PLB, phospholamban; TM-PLB, transmembrane phospholamban; SR, sarcoplasmic reticulum; SERCA, $Ca^{2+}$-ATPase; SDS−PAGE, sodium dodecyl sulfate−polyacrylamide gel electrophoresis; EPR, electron paramagnetic resonance; WT, wild type; FET, fluorescence energy transfer; SSNMR, solid-state nuclear magnetic resonance; CP-MAS, cross-polarization magic-angle spinning; CT-DIPSHIFT, constant time dipolar and chemical shift NMR; DMPC, dimyristoylphosphatidylcholine.

10.1021/bi0482351 CCC: $30.25 
Published on Web 02/16/2005

recent studies have aimed at obtaining information about the oligomeric structure of PLB and its variants in a membrane environment represented by model phospholipid bilayers. Spin-label electron paramagnetic resonance (EPR) has been used to measure the number of lipids in contact with PLB and thus obtain an average oligomeric size of approximately 3.5 units (*3*). Phosphorylation of PLB increases the average size from 3.5 to 5.3 units, an effect that is abolished by high ionic strength (*3*). In separate work using fluorescence energy transfer (FET) measurements it was estimated that the average oligomeric size of PLB is 9−11 units (*4*, *15*). After PLB was incorproated into membranes with $Ca^{2+}$-ATPase, the oligomeric size was reduced to an average of 5 subunits, which is accompanied by a simultaneous increase in the fraction of monomeric PLB from 10% to 30−40% (*4*, *15*).

More detailed insights into the structure and organization of PLB oligomers in lipid bilayers have been provided using solid-state nuclear magnetic resonance (SSNMR) methods. Solid-state deuterium NMR experiments have shown that, of three Leu residues (42, 43, and 44) in the transmembrane domain, L42 is oriented toward the surrounding lipids, while L43 and L44, both of which are sensitive to mutation, are oriented toward the helix interfaces (*16*). This provides further evidence that pentameric stabilization of PLB is the result of Leu/Ile packing. Solid-state NMR studies have also provided local details of the molecular structure of PLB when reconstituted into lipid membranes. These suggest that the wild-type protein forms a continuous α-helix (*17*), whereas in the null-cysteine analogue the transmembrane and cytoplasmic domains of the protein are approximately perpendicular to each other (*18*).

In a recent study by Thomas and co-workers, spin-label EPR was used to examine the oligomeric potential of the null-cysteine PLB analogue (Ala-PLB) incorporated into lipid bilayers (*19*). The behavior of Ala-PLB was compared with the properties of a related peptide consisting of residues 26−52 (i.e., the transmembrane domain) of the null-cysteine PLB (TM-Ala-PLB) (*17*). SDS−PAGE analysis showed that the oligomeric state of TM-Ala-PLB was found to be dependent on the amount of protein, requiring 40 $\mu$g of peptide for pentamer formation (*19*). By contrast, Ala-PLB remained predominantly monomeric on SDS−PAGE gels at all concentrations. EPR measurements of spin-labeled lipids in contact with the PLB analogues in lipid bilayers suggested that the oligomeric states of the analogues reflected their behavior in SDS micelles, with TM-Ala-PLB having a much greater tendency to aggregate than Ala-PLB (*19*). These results imply that the stability of the PLB pentamer in lipid bilayers is due primarily to attractive interactions between transmembrane domains overcoming the repulsive electrostatic forces between the cytoplasmic domains (residues 1−25) (*19*).

In the work described here, SSNMR spectroscopy has been used to examine in more detail the oligomeric behavior of Ala-PLB and TM-Ala-PLB in phospholipid membranes by measuring their rates of rotational diffusion. The PLB analogues were site-specifically labeled in the transmembrane region with nonperturbing $^2$H and $^{13}$C probes to enable direct observation of the proteins in lipid bilayers. From the analysis of wide line $^2$H NMR line shapes for the labeled proteins, and with new interpretations of $^{13}$C−$^1$H dipolar interactions under magic-angle spinning conditions, it was possible to resolve two protein species of both Ala-PLB and TM-Ala-PLB. The two species differed in their rates of rotational diffusion, as would be expected for a mixture of different-sized oligomers or oligomers and monomers. These results indicate that the analysis of the PLB variants on SDS−PAGE gels is unreliable as a predictor of the aggregation potential of these polypeptides in a membrane environment.

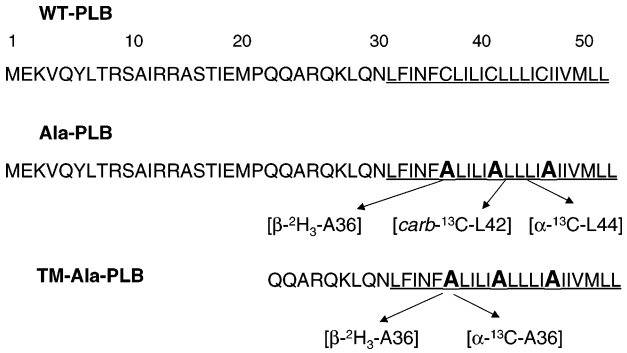


FIGURE 1: Summary of the sequences of phospholamban (PLB) and the null-cysteine variants Ala-PLB and TM-Ala-PLB showing the positions of the mutations (in bold) and isotope labels for NMR analysis. Alanine-substituted variants were prepared with labels at the sites shown to give samples of Ala-PLB and TM-Ala-PLB each containing a single $^{13}$C label at an α-carbon site or three $^2$H labels at an alanine $\beta$-position and an additional sample of Ala-PLB doubly labeled with $^{13}$C at carbonyl and α-carbon sites.

## EXPERIMENTAL PROCEDURES

*Materials.* Synthetic, isotope-labeled PLB analogues were purchased in pure form (>95%) from the Department of Biochemistry, University of Southampton. The sequence of the PLB analogues and the positions of the labels are illustrated in Figure 1. One analogue was a null-cysteine variant of PLB in which the native cysteine residues (C36, C41, C46) were replaced by alanine. The triple mutant is referred to as Ala-PLB in accord with the nomenclature of Thomas and co-workers (*19*). Ala-PLB was labeled either with three deuterium atoms at the $\beta$-position of residue 36 of wild-type PLB ([$\beta$-$^2$H$_3$-A36]Ala-PLB), with a $^{13}$C label at the α-position of residue 44 in native PLB ([α-$^{13}$C-L44]Ala-PLB), or with $^{13}$C labels at both the α-position of Leu44 and the carbonyl of Leu42 ([*carbonyl*-$^{13}$C-L42,α-$^{13}$C-L44]Ala-PLB). In addition, a peptide corresponding to the transmembrane helix of PLB (residues 23−52) was prepared with the three native cysteine residues replaced by alanine. This peptide is referred to here as TM-Ala-PLB, again for consistency with the nomenclature of Thomas and co-workers (*19*), although our peptide sequence is three residues longer than the peptide of the previous work. TM-Ala-PLB was labeled with three deuterium atoms in the side group corresponding to residue 36 of native PLB ([$\beta$-$^2$H$_3$-A36]TM-Ala-PLB). A $^{13}$C-labeled TM-Ala-PLB sample was available to us from previous studies, which contained the label at the α-position of residue 36 ([α-$^{13}$C-A36]TM-Ala-PLB. The position of the $^{13}$C label in TM-Ala-PLB therefore does not correspond to the position of the $^{13}$C-labeled site in Ala-PLB. The exact alignment of the labels in the two proteins was not considered necessary to compare the NMR measurements of rotational diffusion for the two species. In both cases the $^{13}$C labels lie within the well-defined transmembrane helical regions, which are likely to rotate as rigid body

cylinders. It is reasonable to assume, therefore, that the different $^{13}$C-labeled sites are equivalent in reporting the rotational mobility of the variants.

Dimyristoylphosphatidylcholine (DMPC) was purchased from Avanti-Polar Lipids Inc. All other chemicals were purchased from Sigma Chemicals Ltd.

*Preparation of Membrane Samples.* DMPC and either TM-Ala-PLB or Ala-PLB were codissolved in 50:50 chloroform−methanol at a molar ratio of 20:1 and dried down to a film under argon followed by further drying under high vacuum overnight. Samples were then rehydrated in 10 mM phosphate, pH 7, and centrifuged at 13000 rpm in a benchtop centrifuge. Subsequent $^1$H NMR analysis confirmed that no residual organic solvent was present in the hydrated samples.

In the early stages of the work, when the method for sample preparation was being developed, the hydrated membranes containing Ala-PLB or TM-Ala-PLB were subjected to density gradient centrifugation to separate proteolipid membranes from protein-free membranes and any aggregated protein not associated with the lipids. Samples were run overnight on 5−40% sucrose gradients, and in each case a single band was obtained at approximately 20% sucrose, demonstrating successful incorporation of the protein into lipid bilayers. The sucrose gradient was fractionated into 1 mL aliquots, and each was analyzed for lipid and protein content. No evidence was found for protein-free lipid fractions or for protein not associated with membranes, indicating that all of the protein was fully incorporated into the lipid bilayer. The $^{13}$C CP-MAS NMR spectrum of the single membrane band isolated from the gradient (not shown) was identical to spectra of samples not subjected to fractionation. The density gradient step was therefore considered unnecessary and omitted from the routine preparation of samples used for all of the NMR experiments shown here.

The freshly prepared hydrated membrane samples were centrifuged in 10 mM phosphate, pH 7, and the resultant pellets were stored at −20 °C until required for NMR. Sample preparation for $^2$H NMR experiments required an extra stage in which the membranes were subjected to three wash cycles. In each wash cycle the pellet was resuspended in 10 mL of 10 mM phosphate, pH 7, in deuterium-depleted water, left on ice for 30 min, and centrifuged at 100000*g* for 30 min.

*SDS−PAGE Analysis.* All synthetic proteins were analyzed by SDS−PAGE (*20*). In the case of TM-Ala-PLB samples were run on Tris−Tricine gels (*21*). Prior to Coomassie staining, TM-Ala-PLB was first stained using an adaptation of a zinc negative stain (*22*). Gels were fixed for 30 min in methanol−$H_2O$−acetic acid (50:48:2 by volume) and then washed in water for 1 h before being incubated in 0.2 M imidazole−0.1% SDS for 5 min. After beng washed further in water, the stain was developed in 50 mM zinc chloride.

*NMR Measurements.* All solid-state NMR experiments were performed on a Bruker Avance 400 spectrometer operating at a magnetic field of 9.3 T and corresponding to resonance frequencies of 400 MHz for $^1$H, 100 MHz for $^{13}$C, and 62 MHz for $^2$H. Proton-decoupled $^{13}$C CP-MAS experiments were performed by rotating the sample at the magic angle in a 4 mm zirconia rotor at rates $\nu_r$ of between 4 and 7 kHz. Hartmann−Hahn cross-polarization from $^1$H to $^{13}$C was achieved over a 1.6 ms contact time at a field of 65 kHz for both nuclei, and protons were decoupled during signal acquisition at a field of 85 kHz. A recycle delay of 2 s was used in all $^{13}$C CP-MAS experiments. In some experiments, Hartmann−Hahn cross-polarization (i.e., the $^1$H 90° pulse and $^1$H/$^{13}$C contact period) was replaced with a single 4 $\mu$s 90° pulse at the $^{13}$C frequency for direct excitation. In these experiments the recycle delay was 10 s. The sample temperature was maintained between −10 and 30 °C (±0.5 °C).

Measurements of $^{13}$C−$^1$H dipolar coupling strengths were performed using the constant time dipolar and chemical shift (CT-DIPSHIFT) correlation experiment (*23*) at a spinning frequency $\nu_r$ of 7 kHz. In this experiment, $^1$H−$^{13}$C Hartmann−Hahn cross-polarization or direct excitation of $^{13}$C was first achieved under the conditions described above. The $^{13}$C magnetization was then allowed to evolve as a spin−echo over two rotor cycles ($2/\nu_r$), applying an 8 $\mu$s $\pi$ pulse to the $^{13}$C spins between the two rotor cycles to refocus the chemical shifts. Homonuclear decoupling of protons was applied for a defined interval $t$ during the first rotor cycle of the dipolar evolution using the frequency-switched Lee−Goldburg sequence. Following the period $t_1$, continuous wave proton decoupling was applied at a field of 85 kHz for a period $2/\nu_r - t$. The $^{13}$C signal was then detected, with two-pulse phase-modulated (TPPM) proton decoupling (*24*) applied at a field of 85 kHz during the acquisition period. In a series of seven experiments, peak intensities were measured for different intervals $t$, where $0 \geq t \geq 1/\nu_r$. Values of the C−H dipolar coupling strength $d_{HC}$ were obtained by comparing simulated curves with the experimental peak intensities at the different intervals.

Rotational resonance (RR) $^{13}$C NMR experiments were performed on [*carbonyl*-$^{13}$C-L42,α-$^{13}$C-L44]Ala-PLB using the standard pulse scheme described elsewhere (*25*). Sample spinning was adjusted to a rate corresponding to the $n = 1$ or $n = 2$ rotational resonance conditions. The $n = 1$ RR condition is attained when the sample spinning rate is equal to the frequency ($\Delta\nu$) separating the α-carbon and carbonyl resonances, and the $n = 2$ RR condition is met when the MAS rate is half the value of $\Delta\nu$. The $n = 1$ RR condition corresponded to frequencies of 12058 Hz for species 1 and 12184 Hz for species 2. After cross-polarization under the conditions described above, the $^{13}$C magnetization was returned to the *z*-axis by a nonselective 4 $\mu$s 90° pulse. The carbonyl $^{13}$C magnetization was then selectively inverted using a DANTE pulse train. Magnetization was allowed to exchange over a mixing period of between 1 and 40 ms, followed by a nonselective 4 $\mu$s 90° read-out pulse. Protons were irradiated at a field of 85 kHz using TPPM decoupling (*24*) throughout the mixing period and signal acquisition. The experimental temperature was −20 °C. The experimental points were compared with simulated curves, which are computed as a function of $^{13}$C−$^{13}$C internuclear distance, relative tensor orientations, and the zero-quantum relaxation time ($T_2^{ZQ}$), which was estimated from the carbonyl and α-carbon peak widths ($\Delta\nu_{CO}$ and $\Delta\nu_\alpha$) according to $T_2^{ZQ} = 1/\pi(\Delta\nu_{CO} + \Delta\nu_\alpha)$ (*25*).

Nonspinning, wide line $^2$H NMR experiments were performed with a single tuned probe head fitted with a 5 mm horizontally oriented coil. The quadrupole echo experiment ($90_x-t_1-90_y-t_2-$acquire) described by Davis (*26*) was used with an interpulse delay $t_1$ of 22 $\mu$s, a preacquisition delay $t_2$ of 20 $\mu$s, a $\pi/2$ pulse length of 3.5 $\mu$s, and a recycle

delay of 1 s. Nonspinning, wide line $^{31}$P NMR spectra of the DMPC headgroups were recorded for each sample before and after $^{2}$H and $^{13}$C spectra were collected to confirm that the membranes remained in the lamellar phase throughout. No evidence was found for substantial (>5%) nonbilayer lipid components in any of the membrane samples.

## THEORY

*General Approach.* The aim of this work was to gain information about the oligomeric states of Ala-PLB and TM-Ala-PLB from measurements of rates of protein rotational diffusion. The correlation time describing the rate of rotational diffusion of a cylindrical (i.e., helical) transmembrane domain of a bilayer spanning protein can be expressed as (*27*)

$$\tau_R = \frac{2\pi\eta d^2 h}{3kT} \quad (1)$$

where $d$ is the diameter of the protein, $h$ is the height of the transmembrane domain, $\eta$ is the membrane viscosity (2.4−5 P), $k$ is the Boltzmann constant, and $T$ is temperature. Hence the diameter of a protein can, in principle, be estimated if $\tau_R$ is measured experimentally. In SSNMR spectroscopy, the rate of rotational diffusion of a protein can have a scaling effect on the observable interactions of its nuclear spins, including $^{13}$C−$^{1}$H dipole−dipole interactions and quadrupolar interactions. With suitable isotope labeling, experimentation, and analysis of the data it is possible, therefore, to relate the scaling effect to rates of rotational diffusion. The theory relating the experimental measurements to rotational correlation times is described in the following two sections.

*Calculation of Correlation Times from $^{2}$H NMR Spectra.* The line shapes of $^{2}$H NMR spectra from $CD_3$-labeled Ala-PLB and TM-Ala-PLB in lipid bilayers are sensitive to molecular rotational diffusion on the microsecond time scale, which scale the observed magnitude of the deuterium quadrupolar interaction. In the absence of motion other than the rotation of the $CD_3$ group about the C−C bond, the quadrupole coupling constant ($e^2qQ/2h$) is scaled from a typical value of ∼170 kHz to ∼57 kHz by rapid rotation of the deuteriomethyl group about the 3-fold axis of symmetry. This scaled value can be read directly from the $^{2}$H line shape from the separation of the two most intense lines (the quadrupole splitting $\Delta\nu_Q$). In the presence of rotational diffusion, the quadrupole coupling constant is scaled further by molecular motion, and experimental $^{2}$H NMR spectra must be compared with simulated spectra to gain insight into the motional behavior of the polypeptides in phospholipid bilayers.

Simulations of NMR line shapes were based on models of a transmembrane helix undergoing two modes of anisotropic rotation about its long axis at different rates. The helix reorientation was simulated either as a two-site exchange process, in which the peptide flips between two equally populated symmetry-related rotomers, or as a continuous rotation model, which was approximated as jumps between three equally populated symmetrical rotomers. The calculations must take into consideration the angular dependence of the quadrupolar interactions for individual $CD_3$ groups in a spherically weighted powder distribution of bilayer-embedded peptides. The orientation of the unique component of the electric quadrupole coupling tensor $V_{zz}$ is transformed from the principal axis system (PAS) through a series of intermediate frames to the laboratory frame. Using the convention of Brown et al. (*28*), the quadrupole splitting for a single molecular orientation $i$ is given by

$$\Delta\nu_Q = \frac{3}{2}\left(\frac{e^2qQ}{h}\right)D_{00}^{(2)}(\Omega_{PL}) \quad (2)$$

where

$$D_{00}^{(2)}(\Omega_{PL}) = \sum_j\sum_k D_{0j}^{(2)}(\Omega_{BL})D_{jk}^{(2)}(\Omega_{MB})D_{k0}^{(2)}(\Omega_{PM}) \quad (3)$$

in which $D_{mn}^{(2)}(\Omega_{XY})$ are elements of the second-order Wigner rotation matrix for the transformation from frame X to frame Y, $\Omega_{XY}$ represents the set of Euler angles $\alpha_{XY}$, $\beta_{XY}$, $\gamma_{XY}$ between the two frames, and $j$ and $k$ take integer values from −2 to +2. The set $\Omega_{PM}$ contains the Euler angles ($\alpha_{PM}$, $\beta_{PM}$, $\gamma_{PM}$) relating the PAS to the molecular frame. For an alanine methyl group in a transmembrane helix, $\beta_{PM}$ takes the value 56°, which is the angle between the Cα−C$\beta$ bond of alanine and the long axis of an α-helix. Angles $\Omega_{MB}$ relate the molecular frame to the axis system for the lipid bilayer. Here, $\beta_{MB}$ is the angle between the peptide helical axis and the bilayer normal, which is assumed to be zero on the basis of previous observations (Hughes and Middleton, unpublished work). In the model for a peptide undergoing a two-site symmetrical jump about its rotational long axis, $\Omega_{MB}$ takes values of (0°, 0°, 0°) and (0°, 0°, 180°). In the model for continuous rotation, $\Omega_{MB}$ takes values of (0°, 0°, 0°), (0°, 0°, 120°), and (0°, 0°, 240°). The final transformation from the bilayer frame to the laboratory frame depends on angles $\Omega_{BL}$. Simulations for a powder distribution comprised a superposition of $i$ Pake doublets, each separated by $\Delta\nu_Q$, for $i$ = 64800 random orientations defined by angles $\alpha_{ML}$, $\beta_{ML}$, and $\gamma_{ML}$. The splittings calculated for each orientation were scaled further by an $S_{mol}$ term of 0.9 where appropriate.

The $^{2}$H resonance frequencies ($\pm\omega_i/2\pi$) for each peptide molecule $i$ in the intermediate bilayer frame are therefore modulated by molecular reorientation between the different rotomers. The rotationally modulated frequencies were calculated by the method of Wittebort et al. (*29*), by diagonalization of an $n \times n$ exchange matrix (see below) in which $n$ is the number of sites (2 or 3). The matrix contains as elements the linear combination of resonance frequencies for each rotomer, the relative populations of each rotomer, and the correlation time $\tau_C$ defining the rate of reorientation (explained in more detail in the next section). The entire simulation procedure was carried out using the GAMMA C++ library (*30*).

*Calculation of Correlation Times from $^{13}$C−$^{1}$H Couplings.* PLB analogues were prepared with $^{13}$C labels at the α-position of residues in the transmembrane domain. The effect of rotational diffusion on the magnitude of the $^{13}$C−$^{1}$H dipolar coupling constant ($d_{HC}$) at the labeled sites can be measured under MAS conditions using the CT-DIPSHIFT experiment. So-called dipolar curves are obtained by plotting the peak intensities corresponding to the $^{13}$C-labeled site as the magnetization evolves under $^{13}$C−$^{1}$H coupling for different periods up to one cycle of sample rotation. In the usual applications of the CT-DIPSHIFT experiment, the experi-

mental curves are compared with powder-averaged simulations calculated using the theory described by Hong et al. (*23*). The best agreement between the simulated and experimental dipolar curves (determined by minimizing the $\chi^2$ function) provides the value of $d_{HC}$. Here, the couplings may be scaled by molecular motion, and the theory must be adapted to relate the apparent $d_{HC}$ value to the rotational correlation time $\tau_R$ for the PLB analogues.

The calculations were modified to take into account the anisotropic rotation of a peptide according to the two-site and continuous models described in the section above. Calculations for the two-site model are shown in the following. The calculations assume that $^{13}C-^{1}H$ coupling occurs only between bonded spin pairs at the α-position, and longer range couplings are neglected. The time-dependent $^{13}C$ resonance frequencies under the influence of the local proton field and magic-angle spinning are given by

$$\omega_1(t) = d_{HC}\sum_j\sum_k\sum_l D^{(2)}_{0j}(\Omega_{PM})D^{(2)}_{jk}(\Omega^1_{MB})D^{(2)}_{kl}(\Omega_{BR})d^{(2)}_{l0}(\beta_{RL})e^{il\omega_r t} \quad (4a)$$

and

$$\omega_2(t) = d_{HC}\sum_j\sum_k\sum_l D^{(2)}_{0j}(\Omega_{PM})D^{(2)}_{jk}(\Omega^2_{MB})D^{(2)}_{kl}(\Omega_{BR})d^{(2)}_{l0}(\beta_{RL})e^{il\omega_r t} \quad (4b)$$

in which $\omega_1$ and $\omega_2$ are the frequencies at a given time $t$ during the dipolar evolution period $t_1$ (where $t \leq t_1$ and $t_1 \leq 1/\nu_R$) for the two peptide rotomers (denoted by subscripts 1 and 2), $d_{HC}$ is the rigid limit dipolar anisotropy, and $j$, $k$, and $l$ take values from +2 to −2. The Euler angles $\Omega^1_{MB}$ in eq 4a take values of (0°, 0°, 0°) and $\Omega^2_{MB}$ in eq 4b take values of (0°, 0°, 180°). The operation $d^{(2)}_{l0}(\beta_{RL})$ transforms from the rotor frame to the laboratory frame, with $\beta_{RL}$ equal to 54.7°. Using the method of Wittebort et al. (*29*) for a two-site jump between equally populated rotomers, the transverse magnetization at a given instant during $t_1$ is expressed by

$$\dot{M}(t) = \sum_{n=1}^{2}(i\omega_i(t)\delta_{ij} + R_{ij})M_n \quad (5)$$

where, for two equally populated sites in the two-site exchange model, the $R_{ij}$ terms are related to the rotational correlation time $\tau_R$ according to

$$R_{12} = R_{21} = {\tau_R}^{-1} \quad (6a)$$

$$R_{11} = R_{22} = -{\tau_R}^{-1} \quad (6b)$$

The matrix $i\mathbf{w} + \mathbf{R}$ is diagonalized to give the eigenvalue matrix $\lambda$ containing the frequencies after exchange. The MAS phase angles accumulated during the dipolar evolution time $t$ are given by

$$\lambda_n(t) = \int_0^{t_1}\lambda_n\,dt \quad (7)$$

and the observed $^{13}C$ magnetization $M(t_1)$ after the dipolar evolution period $t_1$ is written as

$$M(t_1) = \frac{\mathrm{Re}\{e^{\lambda_1} + e^{\lambda_2}\}}{2} \quad (8)$$

The simulations were performed with powder averaging for 5000 crystallites by randomly generating the Euler angles $\Omega_{BR}$ that transform from the bilayer frame to the rotor frame. A similar procedure was adopted for the continuous rotation (i.e., three-site) model, in which frequencies $\omega_1$, $\omega_2$, and $\omega_3$ were calculated from Euler angles $\Omega^1_{MB}$ of (0°, 0°, 0°), (0°, 0°, 120°), and (0°, 0°, 240°). The simulated dipolar curves were finally divided by an exponential function to remove relaxation terms in the eigenvalue matrix arising from exchange broadening.

Simulations of $^{2}H$ NMR spectra and dipolar curves for a transmembrane helical peptide undergoing two-site exchange or continuous rotation at different rates of rotational motion are shown in Figure 2. The spectra and dipolar curves for both models are sensitive to rotational diffusion when the correlation times $\tau_R$ for molecular motion fall between 100 μs (i.e., the rigid limit) and 1 μs (i.e., the fast diffusion limit). For both models of rotation, as the rate increases from the rigid limit to within the intermediate motional range, the amplitudes of the dipolar curves are attenuated while the $^{2}H$ NMR line shapes gain intensity in the central region. At the fast diffusion limit no further change in the $^{2}H$ line shape or the dipolar curves is observed. At the fast limit, continuous rotational motion of the peptide almost completely averages the quadrupolar and C−H dipolar interactions to zero. Consequently, a single narrow line is observed in the $^{2}H$ NMR spectrum (Figure 2c), and in the dipolar profile the $^{13}C$ peak intensities are constant over one rotor cycle (Figure 2d). For two-site jumps at the fast diffusion limit, the $^{2}H$ NMR spectrum and dipolar profiles reflect incomplete motional averaging of the quadrupolar and dipolar anisotropies (Figure 2a,b).

## RESULTS

*Oligomeric Behavior of PLB Analogues on SDS−PAGE Gels.* The null-cysteine phospholamban variants, Ala-PLB and TM-Ala-PLB, were examined by SDS−PAGE to assess their propensities to self-associate within SDS micelles. The Coomassie-stained gel of Ala-PLB (Figure 3a) shows a single band close to the position expected for monomeric protein (marked as ×1 next to the gel). No evidence was found for very high molecular weight (i.e., larger than pentameric) aggregates, which would be indicated by staining of protein unable to enter the 10% separating gel. Hence full-length null-cysteine PLB remains monomeric in SDS in agreement with previous findings (*19*, *31*). Gels of TM-Ala-PLB are shown in Figure 3b. The Coomassie-stained gel of TM-Ala-PLB shows a single band (Figure 3b, middle lane), but the zinc negatively stained gel reveals a distribution of molecular weight species (Figure 3b, right lane). The expected distances run for the monomeric, dimeric, and pentameric forms of TM-Ala-PLB are marked (as ×1, ×2, and ×5) alongside the gels in Figure 3b. Although the locations of the bands do not correspond exactly to the expected positions, the gels suggest that oligomeric TM-Ala-PLB is present predomi-

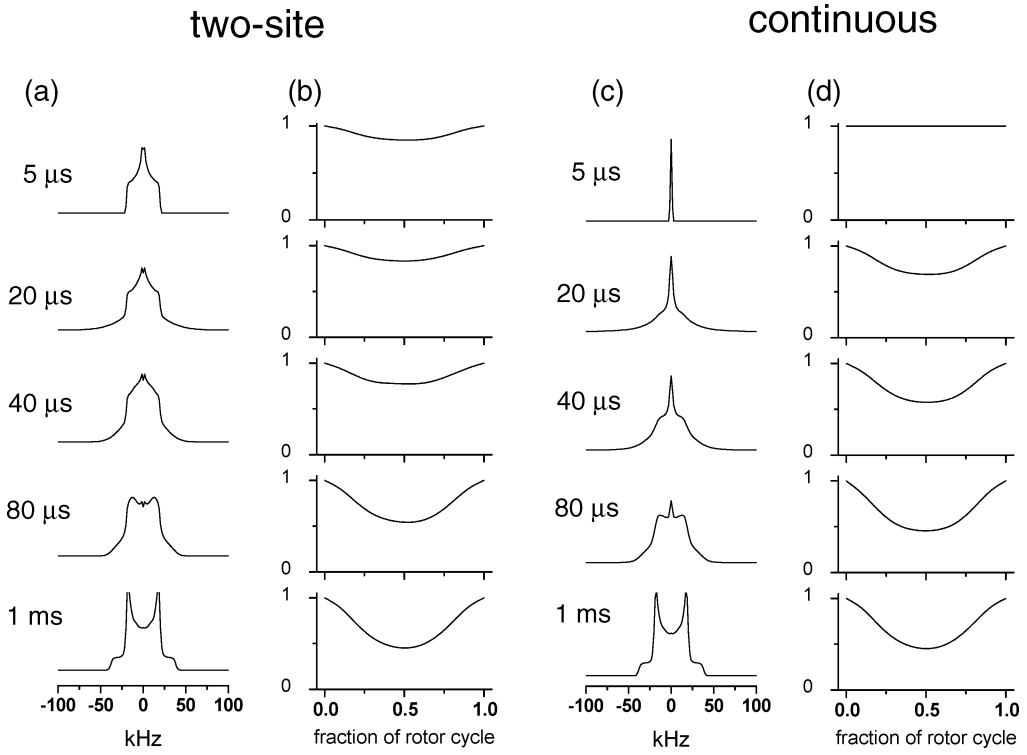


FIGURE 2: Simulations of $^2H$ NMR quadrupolar line shapes (a and c) and $^{13}C-^1H$ dipolar curves (b and d) for a helical transmembrane peptide undergoing 180° rotations between two rotomer states (left) or undergoing continuous rotation (right) at rates described by the correlation times shown. The rotational axis is assumed to be the helical long axis of the peptide, which is parallel with the bilayer normal. The $^2H$ line shape simulations are based on the geometry for a $\beta$-$^2H_3$-labeled alanine residue, and the dipolar profiles are based on the geometry for alanine labeled with $^{13}C$ at the α-position. The simulation procedures are described in the Theory section.

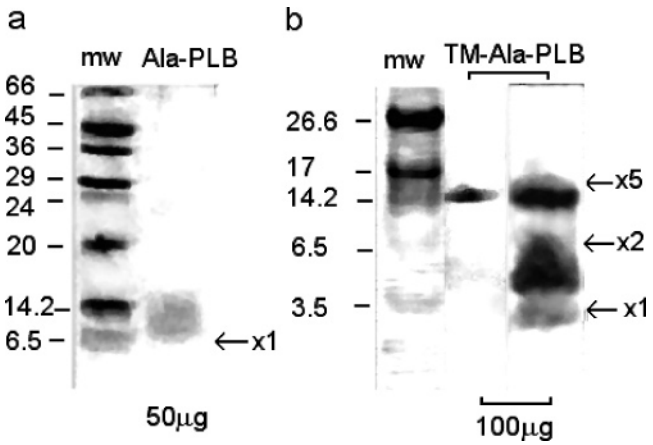


FIGURE 3: SDS−PAGE gels of Ala-PLB (a) and TM-Ala-PLB (b). Ala-PLB was run using standard SDS−PAGE and TM-Ala-PLB using the Tris−Tricine method. The gel of Ala-PLB was Coomassie stained, and gels of Ala-TM-PLB were stained using either Coomassie (b, middle lane) or zinc negative stain (b, right-hand lane). Low-range (66, 45, 36, 29, 24, 20, 14.2, 6.5) and ultra-low-range (26.6, 17, 14.2, 6.5, 3.5) molecular weight markers were used, with the expected distance run for each oligomeric species indicated (monomer, ×1; dimer, ×2; pentamer, ×5).

nantly as pentamers and dimers, with only a small fraction remaining monomeric. The discrepancy between the observed and predicted positions of the bands may be due to the effects of the peptide dimensions, which also determine the mobility of proteins in SDS−PAGE.

*$^{13}C$ CP-MAS NMR Studies of PLB Analogues in Lipid Bilayers.* SSNMR methods were employed to measure the rates of rotational diffusion of Ala-PLB and TM-Ala-PLB within DMPC membranes and to examine how their oligomeric states in lipid bilayers compare with their molecular weight distributions in SDS micelles. Preliminary qualitative information about the peptides was obtained from high-resolution $^{13}C$ CP-MAS NMR spectra of membranes containing PLB variants with $^{13}C$ labels placed at α-carbon sites in the transmembrane region according to the schemes shown in Figure 1.

In Figure 4a−c are shown regions of spectra obtained from membranes containing 5% [α-$^{13}C$-L44]Ala-PLB (i.e., at a lipid/protein molar ratio of 20:1). The spectrum of a freshly prepared membrane sample at −10 °C (Figure 4a) exhibited a single peak at 56 ppm from the PLB variant (defined as $P_1$). However, after incubation of the membrane sample overnight at 4 °C a new peak emerged at 51 ppm (defined as $P_2$) in addition to the peak at 56 ppm (Figure 4b). The relative intensities of the two peaks, $P_1$ and $P_2$ (approximately 2:1), remained constant when the sample was incubated for longer periods. The spectra suggest, therefore, that a single species of Ala-PLB (defined as species 1) is present in the membrane sample initially and that another species (defined as species 2) emerges over a 12 h period. When the NMR experimental temperature was raised to 30 °C, well above the lipid chain melting temperature of ∼23 °C, the spectrum of the same sample retained peak $P_2$, but the original peak $P_1$ at 56 ppm was no longer present (Figure 4c). The spectral changes between −10 and 30 °C were fully reversible, and the initial peak $P_1$ returned when the sample was frozen again.

The disappearance of peak $P_1$ in the CP-MAS spectrum at 30 °C may be linked to an increase in the rotational mobility of the protein species 1 in the fluid-phase lipid bilayers, which interferes with Hartmann−Hahn cross-

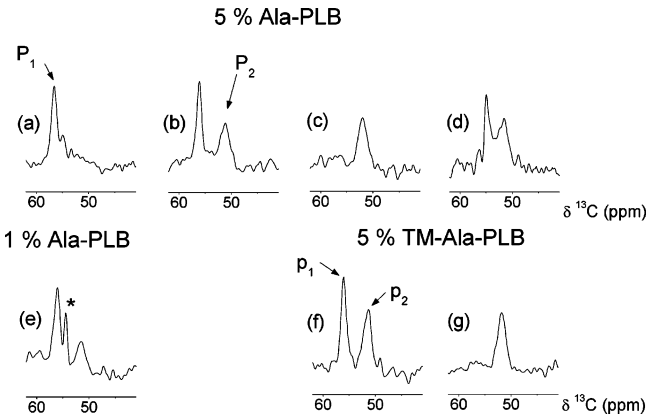


FIGURE 4: Proton-decoupled $^{13}C$ MAS NMR spectra of phospholamban analogues in DMPC membranes at a lipid to protein molar ratio of 20:1 (5% protein) or 100:1 (1% protein). All membrane samples contained 5 mg of protein. A CP-MAS spectrum of 5% [α-$^{13}C$-L44]Ala-PLB recorded at −10 °C immediately after preparation of the membrane sample showed a single peak ($P_1$) from the protein at 56 ppm (a). The membrane sample was incubated at 4 °C for 12 h, and the CP-MAS spectrum recorded again at −10 °C (b) exhibited a new peak at 51 ppm ($P_2$). At 30 °C peak $P_2$ remained in the CP-MAS spectrum, but peak $P_1$ disappeared (c). A direct excitation (DE) $^{13}C$ difference spectrum of the same sample at 30 °C exhibited the two peaks $P_1$ and $P_2$ at 30 °C, although $P_1$ had moved slightly upfield to 55 ppm (d). The peak denoted with an asterisk arises from the phospholipid headgroup. The CP-MAS spectrum at −10 °C from a sample of 1% [α-$^{13}C$-L44]Ala-PLB in DMPC membranes also exhibited peaks $P_1$ and $P_2$ (e). A CP-MAS spectrum of freshly prepared DMPC membranes containing 5% [α-$^{13}C$-A36]TM-Ala-PLB showed two peaks at 56 ppm ($p_1$) and 51 ppm ($p_2$) at −10 °C (f), and peak $p_1$ disappeared from the spectrum at 30 °C (g). Spectra were obtained after accumulating either 4096 or 8192 transients. The MAS rate was 4 kHz in all experiments.

polarization. To test this theory, a direct excitation (DE) $^{13}C$ MAS spectrum was obtained from the same sample at 30 °C. In this experiment, observable $^{13}C$ magnetization is prepared directly and does not rely upon the transfer of magnetization from protons at the Hartmann−Hahn condition. The high lipid background signal in the DE spectrum was removed by subtracting a similar spectrum of pure DMPC membranes to leave a difference spectrum of the protein alone. The difference spectrum clearly exhibited the two peaks, $P_1$ and $P_2$, from the two protein species (Figure 4d). Peak $P_2$ remained visible at 51 ppm, but peak $P_1$ had moved slightly upfield to 55 ppm. Thus species 1 of Ala-PLB cannot be detected in the CP-MAS spectrum at 30 °C but can be seen in the DE spectrum at the same temperature. An explanation for this observation is that species 1 undergoes rapid rotational diffusion in the membranes at 30 °C, which eliminates the $^{13}C-^{1}H$ dipolar interactions that are necessary to generate the signal in the CP-MAS experiment. Species 1 is observed in the DE spectrum, however, because $^{13}C-^{1}H$ dipolar interactions are not required to generate the NMR signal. That the intensity of peak $P_2$ remains in the CP-MAS spectrum at 30 °C (Figure 4c) suggests that species 2 undergoes slower diffusion than species 1, which preserves the $^{13}C-^{1}H$ dipolar interactions. Such differences in the rates of rotational diffusion of the two species would signify that their sizes were also different, with species 2 being the larger of the two. This theory was tested by conducting more detailed measurements of rotational diffusion shown in the next section.

The protein to lipid molar ratio used in the experiments described above is rather high (1:20) and may correspond to only one to two lipid shells around the transmembrane helix of a PLB protomer. Such a high concentration of Ala-PLB in the membrane might promote self-association even if the aggregation potential of the protein is low, so further measurements were performed on a membrane sample containing a lower concentration (1%) of [α-$^{13}C$-L44]PLB. After overnight incubation of the sample at 4 °C, the spectrum at −10 °C clearly shows peaks from the protein at 56 and 51 ppm with approximately the same relative intensities as observed for the higher protein concentration (Figure 4e). Hence lowering the concentration of PLB in the membrane appeared not to prevent the formation of two species.

Similar $^{13}C$ CP-MAS NMR experiments were conducted on freshly prepared DMPC membranes containing 5% [α-$^{13}C$-A36]TM-Ala-PLB. Unlike the observations on Ala-PLB, the spectra of the transmembrane peptide at −10 °C (Figure 4f,g) exhibited peaks at 51 and 56 ppm (labeled $p_1$ and $p_2$, respectively) in the fresh sample without it being necessary to incubate the sample for a sustained period. As was observed in the spectra of Ala-PLB, the lower field peak $p_1$ disappeared when the temperature was raised to 30 °C.

*Rates of Rotational Diffusion from C−H Couplings.* The rates of rotational diffusion of the two Ala-PLB species were estimated by analyzing C−H dipolar curves obtained using the CT-DIPSHIFT experiment. Samples were incubated at 4 °C overnight to ensure that both species were present in the membranes. The measured rates of rotational diffusion are represented by correlation times, which are denoted here as $\tau_R$ when referring to continuous diffusion and as $\tau_R$* when referring to the two-site exchange process defined in the Theory section.

Dipolar curves for 5% [α-$^{13}C$-L44]Ala-PLB in fluid DMPC membranes at 30 °C were prepared by measuring the intensities of peaks $P_1$ and $P_2$ after allowing the magnetization to evolve for different fractions of a sample rotation cycle under the local dipolar field generated by the α-proton. Values of $\tau_R$ for protein rotation were estimated by comparing experimental points with simulated curves. This approach provides estimates of correlation times rather than precise values because it is assumed that the rotational diffusion of the protein is the dominant modulating influence on the C−H dipolar interaction. Other minor modes of motion, such as wobble about the helical axis, may also modulate the dipolar curves (*32*).

Dipolar curves prepared from the intensities of peak $P_1$ from [α-$^{13}C$-L44]Ala-PLB are shown in Figure 5a. When collecting the data, it was necessary to first obtain dipolar curves under freezing conditions to measure the value of the dipolar coupling constant $d_{HC}$ at the rigid limit of the time scale accessible to the NMR experiment (i.e., when $\tau_R >$ 150 ms). The value of $d_{HC}$ could then be substituted into eqs 4a and 4b when calculating rotational correlation times for the protein times at higher temperatures. In the CT-DIPSHIFT experiment the intensity of peak $P_1$ was measured for different intervals after generating observable $^{13}C$ magnetization by Hartmann−Hahn cross-polarization. The dipolar curve obtained from the membrane sample at −10 °C (Figure 5a, filled circles) was identical to curves obtained at −20 and −30 °C (not shown). Hence a temperature of −10 °C was sufficient to freeze out the motions that would

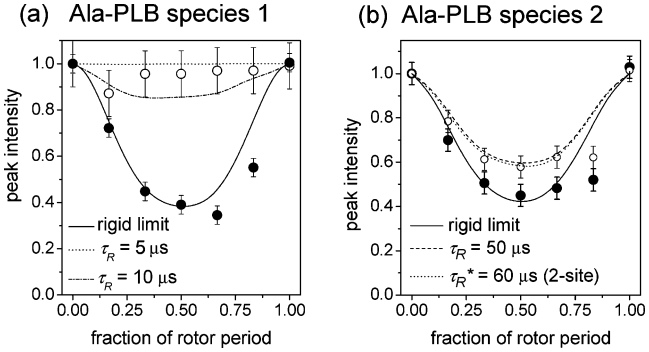


FIGURE 5: $^{13}C-^{1}H$ dipolar dephasing curves for the two observed species of [α-$^{13}$C-L44]Ala-PLB (5%) in DMPC membranes. Points representing peak intensities were measured at −10 °C (●) and 30 °C (○) for seven intervals representing different fractions of one sample rotation cycle. Curves were prepared for species 1 (a) and for species 2 (b) as described in the main text. The experimental points were divided by an exponential function to correct for transverse ($T_2$) relaxation occurring during the dipolar evolution interval. The discontinuous lines represent simulated curves in agreement with the upper and lower error limits of the experimental data at −10 °C and correspond to continuous rotation of the protein at the correlation times shown. The solid line is a simulated curve representing the rigid limit of the spectroscopic time scale (i.e., $\tau_c \geq 150$ μs). Each intensity point was measured from a spectrum obtained after accumulating 4096 transients, and the error bars represent the level of the noise. The MAS rate was 7 kHz.

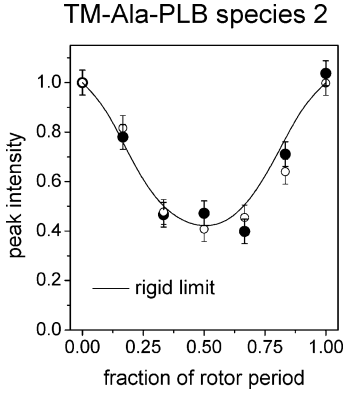


FIGURE 6: $^{13}C-^{1}H$ dipolar dephasing curves for species 2 of [α-$^{13}$C-A36]TM-Ala-PLB (5%) in DMPC membranes. Intensity points were measured at −10 °C (●) and 30 °C (○). Curves were prepared as described in the main text. The solid line represents a simulated curve representing the rigid limit of the spectroscopic time scale. All other conditions were as described for Figure 5.

average the $^{13}C-^{1}H$ dipolar interaction. The experimental points were compared with simulated curves calculated for a rigid molecule at different values of $d_{CH}$, and the best agreement was obtained for a coupling strength of 11 kHz (Figure 5a, solid line). This value is much lower than the predicted rigid limit value of 23 kHz and is attributed to nonideal scaling by the homonuclear decoupling during the evolution period of the experiment (*32*).

Next, a dipolar curve for peak $P_1$ was obtained at 30 °C to examine how the measured $^{13}C-^{1}H$ coupling for this species of [α-$^{13}$C-L44]Ala-PLB was modulated by rotational diffusion of the protein in the fluid lipid membranes. The measurement of dipolar curves at 30 °C was hindered by the inability of CP-MAS to detect peak $P_1$ (cf. Figure 4b). It was necessary, therefore, to make two modifications to the procedure described above. First, to observe peak $P_1$, the CT-DIPSHIFT experiment was conducted using direct excitation rather than cross-polarization to generate observable $^{13}$C magnetization. Second, a parallel series of CT-DIPSHIFT spectra were obtained for both pure DMPC bilayers and DMPC membranes containing [α-$^{13}$C-L44]Ala-PLB under identical conditions. This step was required to obtain difference spectra from which the peaks from the labeled protein could be measured after subtraction of the high natural abundance lipid signals, particularly the choline *N*,*N*′,*N*″-trimethyl resonance at 53.5 ppm. The dipolar curve at 30 °C obtained by this approach is shown in Figure 5a (open circles). The intensity values were compared with simulated curves calculated for different values of correlation times $\tau_R$ (and $\tau_R$*) ranging from 5 μs to 100 μs. Rotational correlation times shorter than 5 μs or longer than 100 μs fall outside the time scale accessible to the spectroscopic measurement. The error bars on the experimental points, which represent the level of the noise, are rather large because of the subtraction procedure. Consequently, a single value for the correlation time could not be measured confidently because curves for a range of values were consistent with the data after taking into account the level of the noise and the accessible spectroscopic time scale. Hence, at 30 °C, species 1 of Ala-PLB undergoes rotational diffusion with correlation time $\tau_R \leq 10$ μs (Figure 5a, dashed line) and possibly faster than the rapid motional limit (i.e., $\tau_R \leq 5$ μs) of the time scale accessible to this approach (Figure 5a, dotted line). The experimental data were not consistent with curves simulated for different rates of rotational diffusion according to the two-site exchange model.

Dipolar curves were also obtained for species 2 of [α-$^{13}$C-L44]Ala-PLB by measuring the intensities of peak $P_2$ at −10 °C (Figure 5b, filled circles) and 30 °C (Figure 5b, open circles). In this case, measurements were conducted using cross-polarization to generate observable $^{13}$C magnetization at both temperatures. At −10 °C the curve was consistent with a coupling strength of 11 kHz, as observed for peak $P_1$ (Figure 5b, solid line). At 30 °C the experimental curve was in closest agreement with simulations for correlation times $\tau_R^* = 60$ μs (Figure 5b, dotted line) and $\tau_R = 50$ μs (Figure 5b, dashed line). Again, it was not possible to confirm the specific mode of rotational diffusion. Hence, the rate of rotational diffusion for the slowly emerging species of Ala-PLB is slower than the rotation of the species initially present in the membranes.

Similar experiments were conducted on 5% [α-$^{13}$C-A36]-TM-Ala-PLB in DMPC membranes (Figure 6). In this case, curves were measured only for peak $p_2$ at 51 ppm (Figure 4e). The curves for the peptide in frozen membranes at −10 °C (Figure 6, filled circles) and fluid membranes at 30 °C (Figure 6, open circles) were virtually identical and in good agreement with the simulated curve for a coupling constant of 11 kHz at the rigid limit (Figure 6, solid line). Hence, the rate of rotational diffusion of this species of TM-Ala-PLB in fluid membranes at 30 °C appears to be slower than the lower motional limit of the spectroscopic time scale (i.e., $\tau_R \geq 150$ μs).

*Estimation of Rates of Rotational Diffusion by $^{2}$H NMR.* Wide line $^{2}$H NMR was used to provide an independent measure of the motional properties of the two Ala-PLB species in DMPC membranes. For this purpose, Ala-PLB was labeled with three deuterons at the alanine methyl group corresponding to residue 36 in the full-length protein.

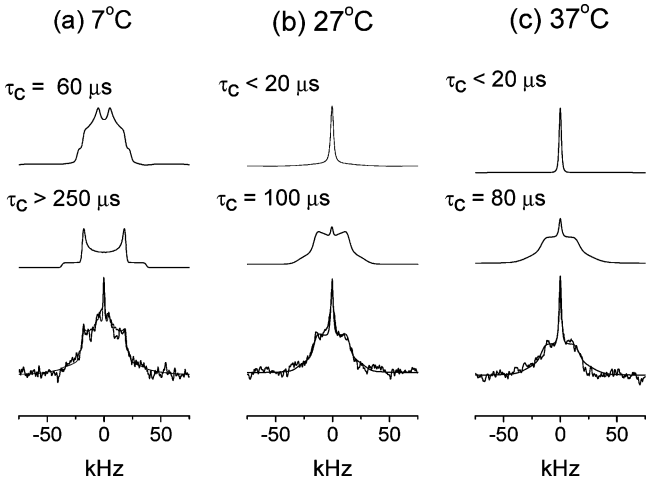


FIGURE 7: Wide line $^2$H NMR spectra of 5% [$\beta$-$^2H_3$-A36]Ala-PLB in DMPC membranes at 7 °C (a), 27 °C (b), and 37 °C (c) shown with overlaid simulated composite line shapes (bottom). The composite simulated lines consisted of two components (shown above the experimental spectra) representing different species of Ala-PLB undergoing relatively fast (top) and slow (middle) rates of rotational diffusion at the correlation times ($\tau_R$ and $\tau_R$*) shown. The two simulated line shapes were combined with a third simulated component representing isotropic HOD/$D_2O$ (not shown) to give the overlaid line shapes. Spectra were obtained after accumulating 100000 transients for 28 h from a membrane sample containing 3 mg of labeled protein.

In Figure 7 are shown $^2$H NMR spectra of DMPC membranes containing 5% [$\beta$-$^2H_3$-A32]Ala-PLB obtained after the sample was incubated overnight at 4 °C. Simulated line shapes are overlaid on the experimental spectra. The line shapes of the spectra are rather complicated and consist of more than one component. Similar $^2$H spectra observed for the transmembrane domain of ErbB-2 in lipid bilayers have been interpreted as representing mixtures of oligomeric and monomeric species (*33*).

The spectrum at 7 °C (Figure 7a, bottom) exhibited an outer component reminiscent of an axially symmetrical quadrupolar interaction, with a quadrupole splitting ($\Delta\nu_Q$) of 37−38 kHz. This component of the line shape resembled the simulated line shape for a peptide undergoing slow rotation with a correlation time $\tau_R$ (or $\tau_R$*) of longer than 250 $\mu$s (Figure 7a, middle). Two central components were also observed. One was a bell-shaped component that was approximated by a simulated line shape for a peptide undergoing two-site rotation with a correlation time $\tau_R$* of 60 $\mu$s (Figure 7a, top). The other, minor, component was a narrow line representing rapid isotropic motion and probably arising from residual HOD/$D_2O$ in the sample. The simulated line shapes representing residual HOD/$D_2O$ are not shown in Figure 7. Combination of the three simulated line shapes provided a good fit to the experimental spectrum (Figure 7a, bottom).

When the temperature was raised to 27 °C (Figure 7b), the outer component became narrower and the overall intensity in the center of the spectrum increased as the broader of the two central lines began to coalesce with the sharp peak attributed to HOD/$D_2O$. The contributions of the two [$\beta$-$^2H_3$-A32]Ala-PLB species to the spectrum at 27 °C were represented by two line shapes simulated for continuous rotation at correlation times $\tau_R$ of $\leq$20 $\mu$s (Figure 7b, top) and 100 $\mu$s (Figure 7b, middle), which when combined with a small component for HOD/$D_2O$ gave a good fit to the spectrum (Figure 7b, bottom). When the temperature was raised further to 37 °C, the inner component of the spectrum was best represented by a line shape for $\tau_R \leq 20$ $\mu$s (Figure 7c, top) and the outer component by a line shape for $\tau_R = 80$ $\mu$s (Figure 7c, middle). It should be noted that correlation times of 20 $\mu$s or shorter cannot be measured reliably from simulations of $^2$H NMR line shapes. This is because, when $\tau_R$ is ~20 $\mu$s, the line collapses to a Lorentzian shape (Figure 2), and further increases in rates of rotational diffusion modulate only the line width (which can be affected by other properties) and not the shape.

In summary, the $^2$H NMR spectra of [$\beta$-$^2H_3$-A32]Ala-PLB at the three temperatures confirm the results of $^{13}$C CP-MAS NMR and indicate that at least two species of Ala-PLB molecules are present in the membrane, which are distinguishable by their relative rotational mobility. These species probably correspond to peaks $P_1$ and $P_2$ in the $^{13}$C CP-MAS spectra (Figure 4). Species 2 undergoes slower rotation in the fluid phase membranes at 30 °C than does the species present initially (species 1). The different motional behavior of the two species indicates that Ala-PLB coexists in different oligomeric states in DMPC bilayers.

*Structural Analysis.* The $^{13}$C CP-MAS NMR spectra of [$\alpha$-$^{13}$C-L44]Ala-PLB and [$\alpha$-$^{13}$C-A36]TM-Ala-PLB reveal a rather large separation of the chemical shifts (5 ppm apart) for the labeled $\alpha$-carbon sites of the two species. Such a marked chemical shift difference might arise if the two species differ in their secondary structures within the transmembrane domains. The average chemical shift value of a Leu $\alpha$-carbon is 57.5 ppm for an $\alpha$-helix, 54.9 ppm for random coil, and 53.9 ppm for a $\beta$-strand (*34*). The average chemical shift value of an Ala $\alpha$-carbon is 54.8 ppm for an $\alpha$-helix, 52.7 ppm for random coil, and 50.8 ppm for a $\beta$-strand (*34*). On the basis of chemical shift values alone it could be suggested that peaks $P_1$ from [$\alpha$-$^{13}$C-L44]Ala-PLB and $p_1$ from [$\alpha$-$^{13}$C-A36]TM-Ala-PLB arise from helical species, while the chemical shifts for $P_2$ and $p_2$ are more consistent with nonhelical structures. An alternative explanation is that the chemical shift difference may reflect the different environments of the $^{13}$C-labeled residues in monomers and oligomers because of helix packing. Experiments were therefore conducted to examine the secondary structures of the two species of Ala-PLB.

The overall secondary structural content of the two Ala-PLB species after incubation overnight was assessed using infrared spectroscopy, by analysis of the amide I and II band frequencies (spectrum not shown). Consistent with previous work on PLB, the spectrum exhibited peaks in the region of 1655 and 1544 cm$^{-1}$, which are typical of the amide I and amide II modes for an $\alpha$-helical structure (*35*). Bands were absent in regions that are indicative of $\beta$-structure (1680−1690 cm$^{-1}$ and 1630−1640 cm$^{-1}$) and random coil (1675 cm$^{-1}$). The infrared spectra are too low in resolution, however, to provide information about what may be only subtle differences in secondary structure around the isotope labeled sites. The local secondary structure of the Ala-PLB species in the transmembrane region was probed further by preparing an analogue labeled with $^{13}$C at the $\alpha$-position of Leu44 and at the carbonyl position of Leu42 ([*carbonyl*-$^{13}$C-L42,$\alpha$-$^{13}$C-L44]Ala-PLB). The linear, through-space distance between the two labels is diagnostic of the local

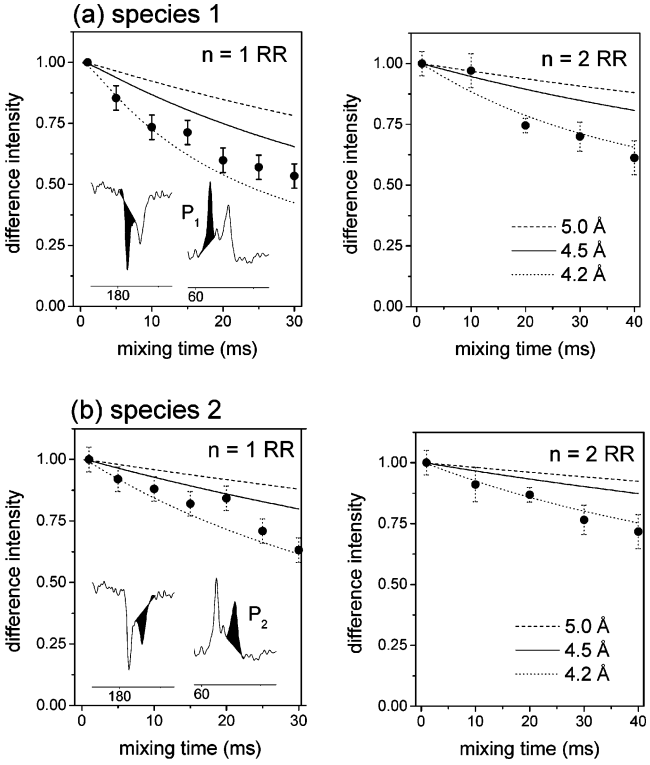


FIGURE 8: Experimental and simulated magnetization exchange curves for species 1 (a) and species 2 (b) of [*carbonyl*-$^{13}$C-L42,α-$^{13}$C-L44]Ala-PLB (5%) in DMPC membranes at the $n = 1$ (left) and $n = 2$ (right) rotational resonance conditions. Curves are plotted as difference magnetization as a function of mixing time. Difference magnetization was measured as the sum of the absolute intensities for the selectively inverted carbonyl peaks and the Cα peaks $P_1$ and $P_2$ for each species. Simulated curves for different $^{13}$C−$^{13}$C distances, 5.0, 4.5, and 4.2 Å, are shown as dashed, continuous, and dotted lines, respectively. The simulated curves were based upon zero-quantum relaxation times of 1.1 ms for species 1 and 0.62 ms for species 2, measured from the line widths of the peaks (inset).

secondary structure: a distance of 4.3−4.5 Å corresponds to a helical structure, and a distance of 5.4 Å corresponds to a $\beta$-sheet. Longer distances are expected for unfolded or extended structures.

The structures of both species 1 and 2 of [*carbonyl*-$^{13}$C-L42,α-$^{13}$C-L44]Ala-PLB in DMPC bilayers were assessed using rotational resonance NMR to measure interatomic distances between the two $^{13}$C-labeled sites in each of the species. This was possible because the peaks for the two species in the carbonyl and α-carbon regions were well resolved from each other (e.g., Figure 8a, inset). The carbonyl spin polarizations for species 1 and 2 were selectively inverted, and magnetization exchange was followed by measuring the difference intensities for the inverted carbonyl peaks and the α-carbon peaks over a mixing period of up to 40 ms. Magnetization exchange was followed at the $n = 1$ and $n = 2$ rotational resonance (RR) conditions corresponding to each of the two species to give a total of four curves (Figure 8).

Magnetization exchange curves of difference intensities are shown for species 1 (Figure 8a) and species 2 (Figure 8b) at $n = 1$ (left) and $n = 2$ (right) rotational resonance. The experimental points are shown with simulated curves calculated for distances of 4.2, 4.5 (the distance expected for a helix), and 5.0 Å. In all of the plots the data for the two species fall largely within the range bounded by curves for 4.2 and 4.5 Å, with few points in the 4.5−5.0 Å range, and no points above the 5.0 Å curve. Although the reliability of the simulated curves is affected to some extent by uncertainties in the estimate of zero-quantum relaxation times ($T_2^{ZQ}$), it is clear that simulated curves for distances of greater than 5 Å (i.e., consistent with nonhelical structures) lie well away from the experimental data. Hence, the rotational resonance experiment suggests that the two species of Ala-PLB are helical within the transmembrane domain around the labeled sites. It should be pointed out, however, that magnetization exchange could take place between the α-carbon and carbonyl sites of adjacent protomer molecules in an oligomeric assembly such as species 2. In such a case, the measured curves would contain contributions from intermolecular and intramolecular magnetization exchange. Molecular modeling of PLB in a pentameric arrangement suggested that the shortest thermodynamically favorable distance between the labeled sites of helices is 5.0 Å and much longer for nonhelical structures. Hence, although the possibility of intermolecular contributions to the data in Figure 8 cannot be ruled out entirely without further, more complicated experiments, such contributions are likely to be significant only when the labeled sites lie within a helix.

## DISCUSSION

The studies described here complement earlier work by Thomas and co-workers, who examined the aggregation state of cysteine-free variants of phospholamban and its transmembrane domain in SDS micelles and in lipid membranes using EPR spectroscopy (*19*). Our SDS−PAGE analysis of the full-length PLB mutant, Ala-PLB, was consistent with the previous work (*19*) and indicated that the protein exists predominantly as a monomer in detergent, with little or no pentamer present. In the previous work the transmembrane domain of TM-Ala-PLB was represented by a peptide comprising residues 26−52 of the intact protein. The version of TM-Ala-PLB used here was slightly larger and comprised residues 23−52 of the native protein. Our observations of the behavior of the transmembrane peptide are in general agreement with the previous work, but with some additional findings. Coomassie-stained SDS−PAGE gels showed that TM-Ala-PLB forms an oligomer in detergent with a molecular weight consistent with a pentameric assembly (Figure 3b). Similar results were found by Thomas and co-workers but using lower amounts of peptide than in our experiments (*19*). In addition, zinc negative staining of the gels has revealed substantial amounts of lower molecular weight species that were not detected by Coomassie staining. The smaller species were consistent with monomers, dimers, or a mixture of both.

In the previous work (*19*) EPR spectroscopy was used to assess the size of Ala-PLB and TM-Ala-PLB in lipid bilayers by estimating the number of boundary lipids surrounding the peptide. The estimate was consistent with an average oligomeric size of 3.3 ± 0.4 protomers, although this value was based upon the assumption that the population of oligomers is homogeneous. Here, solid-state $^{13}$C and $^{2}$H NMR spectroscopy has shown that two species of Ala-PLB are present in DMPC membranes. One species, which is present in freshly prepared membranes, undergoes relatively rapid rotational diffusion ($\tau_R \leq 10$ μs from $^{13}$C−$^{1}$H dipolar

curves) and is possibly monomeric or a small oligomeric assembly. The rotational correlation time of monomeric Ala-PLB has recently been estimated to be ~35 ns from spin-label EPR measurements (*36*), which is well above the fast motional limit ($\tau_R \sim 5$ $\mu$s) of the time scale accessible to the $^{13}C-^{1}H$ dipolar and $^{2}H$ NMR measurements here. Hence the presence of monomer cannot be confirmed by our NMR data alone.

The second species of Ala-PLB is relatively restrained in its rotational motion ($\tau_R \sim 50-60$ $\mu$s) and likely to be an aggregated form of the protein. The formation of the second aggregated species of Ala-PLB is a slow process occurring over a period of 12 h. This observation is consistent with the conclusions of Karim et al. (*19*), who proposed that repulsive forces between the cytoplasmic domains of Ala-PLB combine with the effects of the mutations in the transmembrane domain to prevent oligomerization in lipid membranes. Here, however, it is shown that the process is not prevented, although the rate of aggregation is reduced. In the case of TM-Ala-PLB, the two species appear to exist immediately after the peptide is incorporated into lipid bilayers. The aggregated species of TM-Ala-PLB appears to undergo a slower rate of diffusion ($\tau_R > 100$ $\mu$s) than the slowly emerging aggregated species of Ala-PLB ($\tau_R \sim 50-60$ $\mu$s), suggesting that the repulsive forces between full-length protein results in smaller aggregates than those formed by the transmembrane peptide. Further experiments will be necessary to confirm such a size difference.

It is only possible to speculate about the dimensions of the aggregated species from the NMR data presented here, but it is interesting to compare the rotational correlation times for the PLB analogues with those determined for other integral membrane proteins. Effective correlation times of 60 $\mu$s for the skeletal muscle isoform of the sarcoplasmic reticulum $Ca^{2+}$-ATPase (SERCA1) and 25 $\mu$s for shark rectal fin $Na^{+}/K^{+}$-ATPase (*27*) were determined using spin-label saturation-transfer EPR spectroscopy. Both of these examples are large (>100 kDa) polytopic membrane proteins with 10 transmembrane helices spanning 45 Å and a cytoplasmic domain of 100 Å or so in diameter. Here, the aggregated species of Ala-PLB and TM-Ala-PLB undergo rates of rotational diffusion ($\tau_R > 60$ $\mu$s) comparable to or slower than those observed for $Ca^{2+}$-ATPase and $Na^{+}/K^{+}$-ATPase. It is tempting to suggest, therefore, that the PLB variants form assemblies of comparable diameter than these much larger membrane proteins. Such dimensions are much larger than could be attained by pentamers even of loosely packed helices arranged in a pore-like configuration. One interpretation is that unit cells of pentamers aggregate further into supramolecular assemblies within the membrane. The interactions between pentamers may be weaker than the interactions between protomers within the pentamer unit, which might explain why larger aggregates are not observed on SDS−PAGE gels. This hypothesis must remain untested until more precise data are obtained.

## CONCLUSIONS

The oligomeric state of phospholamban in SR membranes has been a subject of speculation and active investigation for several years. It is generally accepted that a dynamic equilibrium exists between monomers and pentamers in lipid bilayers, but conclusive evidence has been difficult to obtain. Nonconservative substitutions of cysteine residues within the PLB transmembrane domain produce variants that run as monomers on SDS−PAGE gels (*3*, *19*), presumably because the repulsive forces between the cytoplasmic domains of monomers overcome the reduced interactive forces within the transmembrane domain. The effects of such mutations on the oligomeric state of PLB in membrane environments have remained unclear owing to the lack of techniques that are able to directly resolve species of different size in lipid bilayers.

The work described here demonstrates how solid-state NMR data can be interpreted to measure the rotational diffusion of membrane-embedded proteins on the microsecond time scale. Unlike other methods capable of similar measurements, such as saturation-transfer EPR spectroscopy, NMR does not require chemical modifications of the protein with potentially perturbing probes. Moreover, with the NMR approach it has been possible, for the first time, to directly resolve at least two species of the null-cysteine PLB analogue Ala-PLB in lipid bilayers. The different species may be a mixture of monomers and oligomers, or possibly oligomers of various sizes. By contrast, Ala-PLB runs only as a monomer on SDS−PAGE gels. Two conclusions can be drawn from these observations. First, the forces of interaction between the transmembrane domains of the Ala-PLB molecules are sufficient in a membrane environment to overcome the repulsive forces between cytoplasmic domains. Ala-PLB thus remains capable of assembling into oligomers as the molecules diffuse laterally within the lipid bilayer, but the rate of association seems to be rather slow and occurs over a period of hours. The transmembrane cysteine residues do appear to promote and stabilize the oligomers, but probably only as one of several contributions to the overall attractive forces. The second, and more important, conclusion to be drawn is that caution must be exercised when relating the properties of PLB and its analogues in detergent micelles to their state in cell membranes. SDS−PAGE may exaggerate or misrepresent the effect of specific mutations on oligomeric stability in membranes.

## REFERENCES

1. Arkin, I. T., Adams, P. D., Brunger, A. T., Smith, S. O., and Engelman, D. M. (1997) Structural perspectives of phospholamban, a helical transmembrane pentamer, *Annu. Rev. Biophys. Biomol. Struct. 26*, 157−179.
2. Wegener, A. D., and Jones, L. R. (1984) Phosphorylation-induced mobility shift in phospholamban in sodium dodecyl sulfate-polyacrylamide gels—Evidence for a protein-structure consisting of multiple identical phosphorylatable subunits, *J. Biol. Chem. 259*, 1834−1841.
3. Cornea, R. L., Jones, L. R., Autry, J. M., and Thomas, D. D. (1997) Mutation and phosphorylation change the oligomeric structure of phospholamban in lipid bilayers, *Biochemistry 36*, 2960−2967.
4. Li, M., Reddy, L. G., Bennett, R., Silva, N. D., Jones, L. R., and Thomas, D. D. (1999) A fluorescence energy transfer method for analyzing protein oligomeric structure: Application to phospholamban, *Biophys. J. 76*, 2587−2599.
5. Reddy, L. G., Autry, J. M., Jones, L. R., and Thomas, D. D. (1999) Co-reconstitution of phospholamban mutants with the Ca-ATPase reveals dependence of inhibitory function on phospholamban structure, *J. Biol. Chem. 274*, 7649−7655.
6. Autry, J. M., and Jones, L. R. (1997) Functional coexpression of the canine cardiac $Ca^{2+}$ pump and phospholamban in *Spodoptera frugiperda* (Sf21) cells reveals new insights on ATPase regulation, *J. Biol. Chem. 272*, 15872−15880.

7. Kimura, Y., Kurzydlowski, K., Tada, M., and MacLennan, D. H. (1997) Phospholamban inhibitory function is activated by depolymerization, *J. Biol. Chem. 272*, 15061−15064.
8. Arkin, I. T., Adams, P. D., Mackenzie, K. R., Lemmon, M. A., Brunger, A. T., and Engelman, D. M. (1994) Structural organization of the pentameric transmembrane alpha-helices of phospholamban, a cardiac ion-channel, *EMBO J. 13*, 4757−4764.
9. Mayer, E. J., McKenna, E., Garsky, V. M., Burke, C. J., Mach, H., Middaugh, C. R., Sardana, M., Smith, J. S., and Johnson, R. G. (1996) Biochemical and biophysical comparison of native and chemically synthesized phospholamban and a monomeric phospholamban analog, *J. Biol. Chem. 271*, 1669−1677.
10. Karim, C. B., Stamm, J. D., Karim, J., Jones, L. R., and Thomas, D. D. (1998) Cysteine reactivity and oligomeric structures of phospholamban and its mutants, *Biochemistry 37*, 12074−12081.
11. Pollesello, P., Annila, A., and Ovaska, M. (1999) Structure of the 1−36 amino-terminal fragment of human phospholamban by nuclear magnetic resonance and modeling of the phospholamban pentamer, *Biophys. J. 76*, 1784−1795.
12. Simmerman, H. K. B., Kobayashi, Y. M., Autry, J. M., and Jones, L. R. (1996) A leucine zipper stabilizes the pentameric membrane domain of phospholamban and forms a coiled-coil pore structure, *J. Biol. Chem. 271*, 5941−5946.
13. Torres, J., Adams, P. D., and Arkin, I. T. (2000) Use of a new label C-13═O-18 in the determination of a structural model of phospholamban in a lipid bilayer. Spatial restraints resolve the ambiguity arising from interpretations of mutagenesis data, *J. Mol. Biol. 300*, 677−685.
14. Ying, W., and Smith, S. O. (2000) Deuterium NMR reveals helix packing interactions in phospholamban, *Biophys. J. 78*, 924.
15. Reddy, L. G., Jones, L. R., and Thomas, D. D. (1999) Depolymerization of phospholamban in the presence of calcium pump: A fluorescence energy transfer study, *Biochemistry 38*, 3954−3962.
16. Ying, W., Irvine, S. E., Beekman, R. A., Siminovitch, D. J., and Smith, S. O. (2000) Deuterium NMR reveals helix packing interactions in phospholamban, *J. Am. Chem. Soc. 122*, 11125−11128.
17. Smith, S. O., Kawakami, T., Liu, W., Ziliox, M., and Aimoto, S. (2001) Helical structure of phospholamban in membrane bilayers, *J. Mol. Biol. 313*, 1139−1148.
18. Mascioni, A., Karim, C., Zamoon, J., Thomas, D. D., and Veglia, G. (2002) Solid-state NMR and rigid body molecular dynamics to determine domain orientations of monomeric phospholamban, *J. Am. Chem. Soc. 124*, 9392−9393.
19. Karim, C. B., Marquardt, C. G., Stamm, J. D., Barany, G., and Thomas, D. D. (2000) Synthetic null-cysteine phospholamban analogue and the corresponding transmembrane domain inhibit the Ca-ATPase, *Biochemistry 39*, 10892−10897.
20. Laemmli, U. K. (1970) *Nature 227*, 680−685.
21. Schagger, H., and von Jagow, G. (1987) Tricine-sodium dodecyl sulfate-polyacrylamide gel electrophoresis for the separation of proteins in the range from 1 to 100 kDa, *Anal. Biochem. 166*, 368−379.
22. Dzandu, J. K., Johnson, J. F., and Wise, G. E. (1988) Sodium dodecyl-sulfate gel-electrophoresis—Staining of polypeptides using heavy-metal salts, *Anal. Biochem. 174*, 157−167.
23. Hong, M., Gross, J. D., and Griffin, R. G. (1997) Site-resolved determination of peptide torsion angle phi from the relative orientations of backbone N−H and C−H bonds by solid-state NMR, *J. Phys. Chem. B 101*, 5869−5874.
24. Bennett, A. E., Rienstra, C. M., Auger, M., Lakshmi, K. V., and Griffin, R. G. (1995) Heteronuclear decoupling in rotating solids, *J. Chem. Phys. 103*, 6951−6958.
25. Levitt, M. H., Raleigh, D. P., Creuzet, F., and Griffin, R. G. (1990) Theory and simulations of homonuclear spin pair systems in rotating solids, *J. Chem. Phys. 92*, 6347−6364.
26. Davis, J. H., Jeffrey, K. R., Bloom, M., Valic, M. I., and Higgs, T. P. (1976) Quadrupolar echo deuteron magnetic resonance spectroscopy in ordered hydrocarbon chains, *Chem. Phys. Lett. 42*, 390−394.
27. Esmann, M., Horvath, L. I., and Marsh, D. (1987) Saturation-transfer electron-spin resonance studies on the mobility of spin-labeled sodium and potassium-ion activated adenosine-triphosphatase in membranes from *Squalus acanthias*, *Biochemistry 26*, 8675−8683.
28. Petrache, H. I., Dodd, S. W., and Brown, M. F. (2000) Area per lipid and acyl length distributions in fluid phosphatidylcholines determined by H-2 NMR spectroscopy, *Biophys. J. 79*, 3172−3192.
29. Wittebort, R. J., Olejniczak, E. T., and Griffin, R. G. (1987) Analysis of deuterium nuclear-magnetic-resonance line-shapes in anisotropic media, *J. Chem. Phys. 86*, 5411−5420.
30. Smith, S. A., Levante, T. O., Meier, B. H., and Ernst, R. R. (1994) Computer-simulations in magnetic-Resonance—an object-oriented programming approach, *J. Magn. Reson., Ser. A 106*, 75−105.
31. Hellstern, S., Pegoraro, S., Karim, C. B., Lustig, A., Thomas, D. D., Moroder, L., and Engel, J. (2001) Sarcolipin, the shorter homologue of phospholamban, forms oligomeric structures in detergent micelles and in liposomes, *J. Biol. Chem. 276*, 30845−30852.
32. Huster, D., Xiao, L. S., and Hong, M. (2001) Solid-state NMR investigation of the dynamics of the soluble and membrane-bound colicin Ia channel-forming domain, *Biochemistry 40*, 7662−7674.
33. Sharpe, S., Barber, K. R., and Grant, C. W. M. (2002) Evidence of a tendency to self-association of the transmembrane domain of ErbB-2 in fluid phospholipid bilayers, *Biochemistry 41*, 2341−2352.
34. Wang, Y., and Jardetsky, O. (2002) Probability based protein secondary structure identification using combined NMR chemical-shift data, *Protein Sci. 11*, 852−861.
35. Ludlam, C. F. C., Arkin, I. T., Liu, X. M., Rothman, M. S., Rath, P., Aimoto, S., Smith, S. O., Engelman, D. M., and Rothschild, K. J. (1996) Fourier transform infrared spectroscopy and site-directed isotope labeling as a probe of local secondary structure in the transmembrane domain of phospholamban, *Biophys. J. 70*, 1728−1736.
36. Karim, C. B., Kirby, T. L., Zhang, Z., Nesmelov, Y., and Thomas, D. D. (2004) Phospholamban structural dynamics in lipid bilayers probed by a spin label rigidly coupled to the peptide backbone, *Proc. Natl. Acad. Sci. U.S.A. 101*, 14437−14442.


BI0482351